Fast ignitor target studies for the HiPER project[a)]

S. Atzeni,[1,b)] A. Schiavi,[1] J. J. Honrubia,[2] X. Ribeyre,[3] G. Schurtz,[3] Ph. Nicolaï,[3] M. Olazabal-Loumé,[3] C. Bellei,[4] R. G. Evans,[4] and J. R. Davies[5]
[1]*Dipartimento di Energetica, Università di Roma La Sapienza and CNISM, Roma, Italy*
[2]*ETSI Industriales, Universidad Politecnica, Madrid, Spain*
[3]*CELIA, Université Bordeaux 1, CNRS, CEA, Talence, France*
[4]*The Blackett Laboratory, Imperial College, London, United Kingdom*
[5]*Instituto Superior Técnico, Lisbon, Portugal*

(Received 18 January 2008; accepted 20 February 2008; published online 21 April 2008)

Target studies for the proposed High Power Laser Energy Research (HiPER) facility [M. Dunne, Nature Phys. **2**, 2 (2006)] are outlined and discussed. HiPER will deliver a 3ω (wavelength $\lambda=0.35\ \mu$m), multibeam, multi-ns pulse of about 250 kJ and a 2ω or 3ω pulse of 70–100 kJ in about 15 ps. Its goal is the demonstration of laser driven inertial fusion via fast ignition. The baseline target concept is a direct-drive single shell capsule, ignited by hot electrons generated by a conically guided ultraintense laser beam. The paper first discusses ignition and compression requirements, and presents gain curves, based on an integrated model including ablative drive, compression, ignition and burn, and taking the coupling efficiency η_{ig} of the igniting beam as a parameter. It turns out that ignition and moderate gain (up to 100) can be achieved, provided that adiabat shaping is used in the compression, and the efficiency η_{ig} exceeds 20%. Using a standard ponderomotive scaling for the hot electron temperature, a 2ω or 3ω ignition beam is required to make the hot electron range comparable to the desired size of the hot spot. A reference target family is then presented, based on one-dimensional fluid simulation of compression, and two-dimensional fluid and hybrid simulations of fast electron transport, ignition, and burn. The sensitivity to compression pulse shape, as well as to hot electron source location, hot electron range, and beam divergence is also discussed. Rayleigh–Taylor instability at the ablation front has been addressed by a model and a perturbation code. Simplified simulations of code-guided target implosions have also been performed. © *2008 American Institute of Physics*. [DOI: 10.1063/1.2895447]

I. INTRODUCTION

We describe target studies performed in the past 3 years in the framework of the conceptual design of the High Power Laser Energy Research (HiPER) facility. HiPER (Refs. 1 and 2) aims at the demonstration of inertial fusion via fast ignition. It will deliver a 3ω, multibeam, multi-ns-pulse of about 250 kJ and a 2ω or 3ω ignition pulse of 70–100 kJ in a few ps. (Here we indicate with ω the fundamental frequency of the Nd:glass laser, with an *in vacuo* wavelength of 1.053 μm; 2ω and 3ω refer, respectively, to the second and third harmonics, with wavelengths of 0.53 μm and 0.35 μm, respectively.)

We recall that fast ignition[3] is an approach to inertial confinement fusion[4,5] in which an ultraintense driver creates the ignition spark in a precompressed fuel. The separation of the stages of fuel compression and ignition offers the potential advantages of relaxed symmetry and stability constraints, as well as of lower ignition threshold and higher energy gain at lower total driver energy. On the other hand, fast ignition requires efficient coupling of an ultraintense beam to the fuel. Typically, if the fuel density is 300 g/cm^3, this beam has to deliver[6] 15–20 kJ in less than 20 ps into a volume with a radius of about 20 μm and depth of 20–40 μm. According to the original fast ignition scheme, proposed by Tabak *et al.* in 1993,[3] the ignition beam can be created by fast electrons generated by an ultraintense laser pulse. This proposal followed the introduction and development of the chirped pulse amplification technique,[7] making multi-kJ, multi-PetaWatt laser pulses conceivable.[8] However, success of the scheme requires that fast electrons with appropriate energy are efficiently generated, transported from the critical density layer to the compressed fuel, and stopped in a sufficiently small volume of compressed fuel, matching the optimal size of the ignition spark. (For recent reviews addressing these issues, see Refs. 9 and 10.)

A boost to fast ignition was provided by experiments[11,12] using conically guided laser beams: here a hollow cone of a material with high atomic number Z, inserted into an otherwise standard spherical target, provides an open path for the intense beam, which thus produces the hot electrons close to the compressed fuel. It was estimated that 25% of the intense pulse (a few hundred J in 1 ps) heated the compressed fuel. The scheme will soon be tested at higher energy levels at the Omega EP (Ref. 13) (Laboratory for Laser Energetics, LLE, University of Rochester, USA) and the Fast Ignition Realization Experiment[14] (FIREX, Institute of Laser Engineering, Osaka University, Japan) facilities, with intense beams of 2.6 and 10 kJ, respectively (both operating at ω).

HiPER is intended as a subsequent step, demonstrating fast ignition and energy gain. It will take advantage of the results of the above experiments as well as of the experi-

[a)]Paper QI1 1, Bull. Am. Phys. Soc. **52**, 268 (2007).
[b)]Invited speaker.

ments on inertial fusion central ignition to be performed at the National Ignition Facility (Lawrence Livermore National Laboratory, Livermore, USA)[15] and Laser Megajoule (Commissariat a l'Energie Atomique, Bordeaux, France).[16]

The HiPER target concept is based on laser direct-drive compression, followed by cone-guided ultraintense irradiation and subsequent hot electron ignition. First studies on targets for fast ignition demonstration, in the framework of the HiPER project, have been published by some of us. The first paper[17] presented a design space analysis, followed by a conceptual design. It was based on an integrated zero-dimensional gain model, on one-dimensional (1D) simulations of the compression stage, and two-dimensional (2D) model simulations of the ignition and burn stages. (An analogous target study was performed by the LLE group.[18,19]) In another paper[20] aspects of electron transport in the compressed plasma and of electron driven ignition were discussed. A separate publication[21] reviewed issues concerning laser interaction and electron generation and transport.

In this paper, we discuss the present status of HiPER target design. In Sec. II, after summarizing the previous results, we present improved studies of the compression stage, including analyses of Rayleigh–Taylor instability and of sensitivity to pulse shape. We then present model simulations of the hydrodynamics of the implosion of conically guided targets (Sec. III), and simulations of hot electron driven ignition, including improved, realistic treatments of electron transport in the compressed fuel (Sec. IV). These results confirm the general trends of the earlier studies. Concerning compression, ignition at a few hundred kJ requires 3ω light, and accurate temporal shaping of the pulse to spatially shape the shell entropy. The crucial issues, instead, concern ultraintense laser-plasma interaction, electron generation, transport, and energy deposition. Using standard scaling laws for the energy of hot electrons with laser intensity and wavelength, it turns out that achieving ignition and significant energy gain with less than 100 kJ ultraintense laser pulse requires 2ω or perhaps 3ω light, as well as efficient hot electron production and transport to the compressed fuel. In the conclusions (Sec. V) we summarize the main results and also address the limitations of the current studies. Directions of future work and need for experimental studies are also outlined.

II. BASELINE TARGET CONCEPT

In this section, we first discuss general beam and target requirements, leading to a design window in the appropriate parameter space, and then present the 1D study of the current HiPER baseline target concept.

A. Design principles and constraints

General beam requirements are obtained by considering the conditions for fast ignition by a laser-generated electron beam, as well as those for the creation of a fuel assembly with the required density and confinement parameter (areal density) ρR. Here, we refer to simple, single shell spherical targets, ablatively imploded by direct laser irradiation.

Energy, power, and intensity (or, equivalently, energy, beam spot and pulse duration) of the igniting hot electron beam depend on compressed fuel density ρ and electron penetration depth $\mathcal{R}$ in the compressed fuel. In particular, if pulse duration and transverse size take optimal values,[6] ignition is achieved if the delivered energy exceeds[6,22,23]

$$E_{ig} = 18\left(\frac{\rho}{300\ \mathrm{g/cm^3}}\right)^{-1.85} \max\left(1, \frac{\mathcal{R}}{\mathcal{R}_0}\right)\ \mathrm{kJ}, \tag{1}$$

where $\mathcal{R}_0 = 1.2\ \mathrm{g/cm^2}$. The electron penetration, however, is not a free parameter. Electrons are generated by the laser pulse at critical density and then transported to the compressed fuel. Their properties (and then their penetration) will depend on both the laser parameters as well as on the plasma where they are generated and transported. Here, we use a simple, standard model,[22] assuming that the electron temperature (average energy) is related to laser intensity and wavelength by the so-called ponderomotive scaling[24]

$$T_{hot} = \left[\frac{I_{ig}^{laser}}{1.2\times 10^{19}\ \mathrm{W/cm^2}}\left(\frac{\lambda_{ig}}{1.06\ \mu\mathrm{m}}\right)^2\right]^{1/2}\ \mathrm{MeV}, \tag{2}$$

where I_{ig}^{laser} is the igniting laser intensity and λ_{ig} is the laser wavelength. It is worth noticing that the dependence of the electron temperature on laser intensity is not yet fully assessed. Experimental data[25–27] seem to indicate that the hot electron temperature also depends on the parameters of the plasma interacting with the laser light. Simulations by Wilks *et al.*[24] and experimental results by Malka and Miquel[25] agree with Eq. (2), while Beg *et al.*[26] find a weaker dependence on $I\lambda^2$. Computational studies by Wilks and Kruer[28] and by Sentoku[29] show that T_{hot} can be well below the value given by Eq. (2). This occurs if the density scale length at critical density is shorter than the light wavelength and the light interacts with an overdense plasma (which can be the case in cone-guided fast ignition[29,30]).

We also assume the range is proportional to the electron energy according to[3,22]

$$\mathcal{R} = 0.6 f_{\mathcal{R}} T_{hot}\ \mathrm{g/cm^2}, \tag{3}$$

where $f_{\mathcal{R}}$ is a parameter of order unity and T_{hot} is in MeV. We further assume the hot electrons deliver to the compressed fuel a fraction (ignition laser coupling efficiency) η_{ig} of the laser energy, and that the laser beam spot size is equal to the electron beam radius at the compressed fuel, so that $I_{ig} = \eta_{ig} I_{ig}^{laser}$, and $E_{ig} = \eta_{ig} E_{ig}^{laser}$. As a reference value, we take $\eta_{ig} = 0.25$. General expression for the laser energy and intensity required for ignition have been derived in Ref. 17. Here it suffices to give the expression applying to densities and focal spots of planned ignition experiments,

$$E_{ig}^{laser} \geqslant 93\left(\frac{\rho}{300\ \mathrm{g/cm^3}}\right)^{-0.9}\left[\frac{f_{\mathcal{R}}\lambda_{ig}}{0.5\ \mu\mathrm{m}}\frac{0.25}{\eta_{ig}}\right]^2\ \mathrm{kJ}. \tag{4}$$

Laser energy thresholds for fast ignition versus fuel density are plotted in Fig. 1, for $\eta_{ig} = 0.25$ and different values of $f_{\mathcal{R}}\lambda_{ig}$. The thresholds given by Eq. (4) are shown by thick lines. The spot radius is limited to $r_b \geqslant r_{min} = 20\ \mu\mathrm{m}$. We see that ignition with less than 100 kJ requires fuel density $\rho \geqslant 300\ \mathrm{g/cm^3}$ and $f_{\mathcal{R}}\lambda_{ig} \leqslant 0.5\ \mu\mathrm{m}$, i.e., either range short-

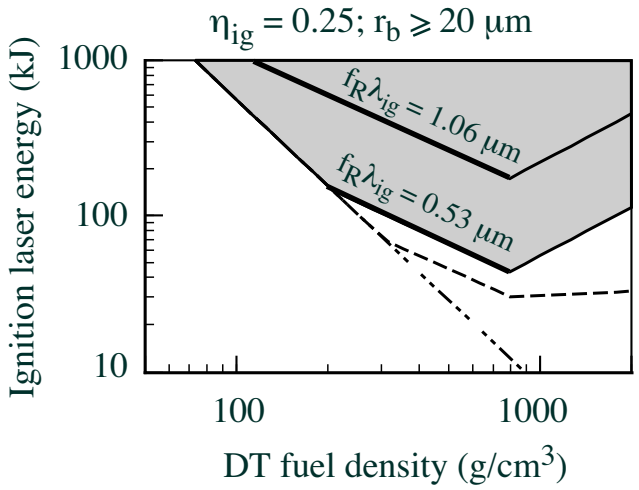

FIG. 1. (Color online) Laser ignition energy E_{ig}^{laser} for hot electron driven fast ignition vs density of the precompressed fuel, for hot spot radius $r_b \geq 20$ μm and different values of the parameter $f_{\mathcal{R}}\lambda_{ig}$ (see labels on the solid curves). It is assumed that the laser beam energy is coupled to the fuel with efficiency $\eta_{ig}=0.25$. The dashed curve assumes range independent of intensity and anyhow shorter than 1.2 g/cm^2; the dotted-dashed line is the ignition scaling law that assumes optimal particle range and optimal beam radius. Adapted from Ref. 17.

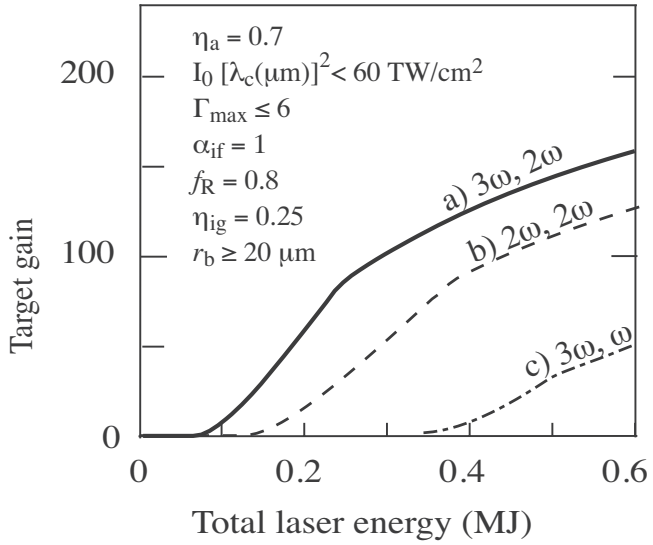

FIG. 2. Gain curves computed by the integrated model. (a) Reference curve, for 3ω compression laser, and 2ω ignition laser; (b) for 2ω compression laser, and 2ω ignition laser; (c) for 3ω compression laser, and ω ignition laser. Values of a few parameters are reported in the figure.

ening and/or laser wavelength of 0.5 μm or shorter. In the following, we shall take $f_{\mathcal{R}}\lambda_{ig}=0.4$ μm as a reference value. [Of course, the above result depends crucially on the use of Eq. (2) for the energy of the hot electrons. If the hot electron temperature is lower than that given by Eq. (2), a longer laser wavelength may be acceptable.]

The compression laser must generate a fuel assembly with peak average density $\langle\rho\rangle_{max}$ in excess of 300 g/cm^3, and with peak confinement parameter $\langle\rho R\rangle_{max}$ exceeding 1–1.5 g/cm^2, as needed for efficient burn.[23] Estimates of the required laser parameters are provided by the scaling laws proposed by Betti and Zhou,[31] which read

$$\langle\rho R\rangle_{max} = \frac{1.46}{\alpha_{if}^{0.55}}\left(\frac{0.35\ \mu m}{\lambda_c}\right)^{1/4}\left(\frac{E_c^{laser}}{100\ kJ}\eta_a\right)^{0.33} \times \left(\frac{u_{imp}}{3\times 10^7\ cm/s}\right)^{0.06} g/cm^2, \quad (5)$$

$$\langle\rho\rangle_{max} = \frac{460}{\alpha_{if}}\left(\frac{I_0}{10^{15}\ W/cm^2}\frac{0.35\ \mu m}{\lambda_c}\right)^{0.13} \times \left(\frac{u_{imp}}{3\times 10^7\ cm/s}\right)^{0.96} g/cm^3. \quad (6)$$

Here, α_{if} is the isentrope parameter of the shell inner layer at the end of the acceleration phase, λ_c, I_0, and E_c^{laser} are the wavelength, intensity, and energy of the compression laser, η_a is the absorption efficiency, u_{imp} is the implosion velocity, and we have assumed that the average density of the igniting fuel is 60% of the peak density.

From Eqs. (5) and (6) we find that the required density and areal density can be achieved by an implosion driven by 100–150 kJ of laser light with wavelength $\lambda_c=0.35$ μm (3ω), at intensity I_0 a few times 10^{14} W/cm^2, if $\alpha_{if}=1$. Increasing the laser wavelength to $\lambda_c=0.53$ μm (i.e., using 2ω light instead of 3ω) would lead to lower areal density and average density (particularly if the intensity is reduced to keep $I_c\lambda_c^2$ constant; see below). This would not only degrade burn, but also increase the energy of the ignition beam [see Eq. (4)].

Gain curves, i.e., estimates of the energy gain as a function of the total laser energy, have been obtained by an integrated model, describing laser driven implosion, density, and pressure multiplication at stagnation, ignition, and thermonuclear burn.[17] The gain curves enforce constrains concerning plasma parametric instabilities, Rayleigh–Taylor instability, and beam focusing. A set of gain curves is shown in Fig. 2. Here the compression laser intensity is constrained by $I_0\lambda_c^2 \leq 6\times 10^{13}$ (W/cm^2) μm^2 in order to limit plasma instabilities.[32] The maximum allowed exponential growth factor (number of e-foldings) for the linear Rayleigh–Taylor instability at the ablation front is set to $\Gamma=6$ (see Chap. 6 of Ref. 4). The electron beam spot is taken as $r_{beam} \geq 20$ μm; furthermore, we have assumed $\eta_a=0.7$, $\eta_{ig}=0.25$, $\alpha_{if}=1$, $f_{\mathcal{R}}=0.8$. The three curves in Fig. 2 are for different wavelengths of the drivers. Curve (a) is for 3ω compression laser and 2ω ignition laser (i.e., $\lambda_c=0.35$ μm and $\lambda_{ig}=0.53$ μm); we also limit the energy of the ignition laser to $E_{ig}^{laser} \leq 100$ kJ. The curve shows that under the above (perhaps optimistic assumptions) ignition can be achieved at total energy of less than 150 kJ, and gain about 100 is obtained at a total energy of 300 kJ. Curve (b) refers to 2ω compression laser and 2ω ignition laser, and shows that the ignition threshold increases to about 200 kJ and the gain lowers. We also observe that in this case the ignition pulse has to deliver about 150 kJ. Finally, curve (c), referring to compression by 3ω and ignition by 1ω light, shows a dramatic increase of the ignition energy and decrease of the gain. All the above curves refer to implosions driven by adiabat-shaping pulses, i.e., laser pulses which keep the entropy of most of the fuel at

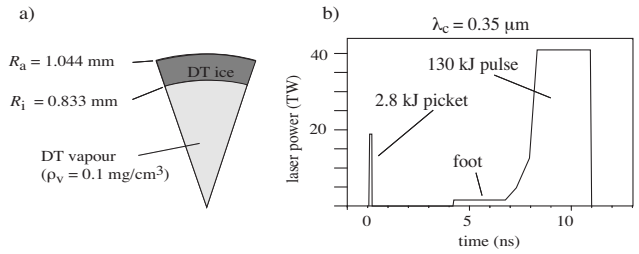

FIG. 3. Baseline target, imploded by a 132 kJ laser pulse: (a) target sketch, (b) laser pulse (notice the adiabat-shaping prepulse). Adapted from Ref. 17.

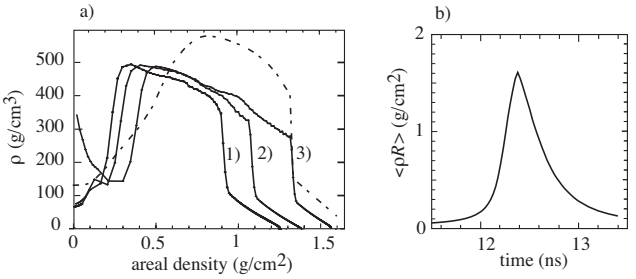

FIG. 4. For the baseline target of Fig. 3: (a) density profiles at times close to maximum compression; solid curves: IMPLO computations (with 2T model and bremsstrahlung loss) at three different times. (1) $t=12.3$ ns; (2) $t=12.325$ ns; (3) $t=12.375$ ns; dashed curve: CHIC computation (with multigroup radiation diffusion) for 200 kJ laser pulse; (b) time evolution of the confinement parameter $\langle\rho R\rangle$ (IMPLO computation).

the desired very low level, but generate higher entropy in the ablator, so as to reduce the growth of the Rayleigh–Taylor instability. Our simple model, supported by simulations, shows that the ignition threshold increases substantially for implosions driven by standard pulses, i.e., without adiabat shaping. A more detailed discussion of the gain curves and an analysis of design parameter space can be found in Ref. 17. Following the results of the present section, in the next section we illustrate the design of targets driven by 3ω light compression pulses of 100–300 kJ, with intensity limited as discussed before, and with the power shaped in time as necessary in order to shape the target adiabat in space.

B. 1D design

The above principles led to the target concept illustrated in Fig. 3. It is a simple all-DT single shell (DT: equimolar deuterium-tritium mixture), driven by a shaped pulse, preceded by an entropy shaping high-intensity picket. (We use the technique of adiabat shaping by type-2 relaxation.[33]) The target is illuminated tangentially by f/18 beams, each with either a parabolic or a super-Gaussian profile. Simulations with the code IMPLO-upgraded,[34] indicated that 0.29 mg of DT are imploded at velocity of about 2.4×10^7 cm/s. The compressed fuel achieves peak density of about 500 g/cm^3. Details are given in Ref. 17.

Concerning the peak confinement parameter $\langle\rho R\rangle_{\max}$, two-temperature (2T) simulations, with bremsstrahlung loss from the central hot gas give $\langle\rho R\rangle=1.57$ g/cm^2, while three-temperature (3T) simulations give $\langle\rho R\rangle_{\max}=1.29$ g/cm^2. In these simulations fusion burn was switched off. If DT burns, and consequently fusion alpha-particle diffusion and energy deposition, are included, $\langle\rho R\rangle_{\max}$ decreases by a further 20%. This is due to preheating of the compressed fuel shell during the final stages of the implosion. We believe this degradation can however be avoided, in several ways. Indeed, experiments[35] and simulations (see Ref. 36, and Sec. III below on cone-guided implosions) show that the central low density gas can be expelled before final shell collapse. In an alternative, one could dope the gas with high-Z elements to increase radiation losses, and then keep it cooler.[37]

Recent simulations of this baseline target with the codes SARA (Ref. 38) (employing multigroup radiation transport by an $S-n$ method) and CHIC (Ref. 39) (with multigroup radiation diffusion) substantially confirm the results obtained with IMPLO and the 3T model. In Ref. 17 we took the 2T simulations (that overestimate the peak confinement parameter $\langle\rho R\rangle_{\max}$) as a reference for the subsequent ignition simulations. However, CHIC and SARA simulations indicate that the same $\langle\rho R\rangle_{\max}=1.6$ g/cm^2 as in IMPLO 2T simulations, and even higher peak density of 550–600 g/cm^3 can be achieved by the same target, by simply increasing the pulse energy from 135 kJ to 180–200 kJ, with a pulse shape similar to that shown in Fig. 3. Figure 4(a)) shows density profiles around maximum compression, obtained by IMPLO (2T model, 135 kJ laser energy) and CHIC (multigroup diffusion, 200 kJ laser energy; but the same can be obtained with about 180 kJ). SARA simulations yield peak density and $\langle\rho R\rangle$ close to CHIC, with a smaller central lower density region. Figure 4(b) shows that the fuel remains confined for a time interval of 100–150 ps.

The reference target and pulse of Fig. 3 can be scaled to larger size and higher energy in a straightforward manner ($E_c\propto M\propto R^3$; $t\propto R$). IMPLO simulations show[17] that the peak density is independent of target size, while $\langle\rho R\rangle_{\max}\propto E^{1/3}$, is in agreement with the scaling proposed in Ref. 31.

The simple model computations of Ref. 17 on the growth of Rayleigh–Taylor instability at the ablation front are substantially confirmed by model simulations with the perturbation code PERLE.[40] For the reference target and pulse of Fig. 3, PERLE computations find an exponential growth factor (number of e-foldings) about 5 for the most unstable modes, with $k\simeq5000$ cm^{-1}. The instability growth rate is higher, and probably unacceptable, for targets driven by pulses without adiabat-shaping picket; in this case, however, PERLE growth factors are more than 20% smaller than those of Ref. 17.

C. Sensitivity to pulse shape

We have studied the sensitivity of peak compression quantities to changes in the pulse shape.[41] We have varied power and duration of the foot, of the ramp, and of the final main-pulse flat-top, as well as the delay between picket and foot. We have varied one parameter at a time, while keeping the laser energy constant. The main effect of these variations is the change of shock timings, and hence in the inner fuel adiabat and consequently, in the fuel compressibility. Figure 5 shows the variation of peak density and $\langle\rho R\rangle_{\max}$ (normalized to the respective optimal values), versus the variation of

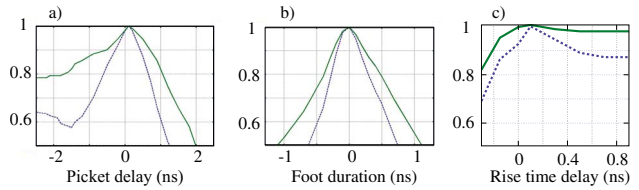

FIG. 5. (Color online) Sensitivity of baseline target compression to changes in the laser pulse. Frames (a)–(c) show, respectively, the relative changes of the peak density (dashed) and peak areal density (solid) vs the timing of the entropy-shaping picket, of the foot duration, and the rising time of the main pulse.

pulse parameters. It turns out that ±250 ps variations of foot delay, foot duration, and rise time imply less than 10% decrease of both peak density and peak areal density. In general, peak density is more sensitive than peak areal density to pulse timing.

III. CONE-GUIDED IMPLOSION

The previous results concern spherically symmetric targets. However, the HiPER baseline target concept is a cone-inserted target. In this section we present our first 2D model simulations concerning such targets. We have studied the late stage of the implosion with the codes SARA-2D (Ref. 38) and POLLUX.[42] A sample SARA simulation is shown in Fig. 6. It refers to a shell similar to that considered in the previous section, with an inserted gold cone. The implosion has first been simulated by the 1D version of SARA. When the shell is approaching the target center (outer shell radius around 300 μm), the 1D profiles are remapped onto a 2D SARA Eulerian mesh and calculations are continued with the cone inserted. Radiation is not included in this simulation. A sequence of snapshots of the shell evolution is shown in the figure. It is worthwhile noticing that the shell collapses in a nearly spherical blob [see Fig. 6(c)], pushing away the DT gas located at the center, and reaching somewhat higher peak density and $\langle \rho R \rangle_{\max}$ than without the cone. This configuration is obtained when a polar P_1 asymmetry is imposed on the implosion velocity, i.e., the implosion velocity is maximum in front of the cone and minimum at the cone surface. Otherwise, the imploded core would have a horseshoe-shaped configuration, reaching a substantially lower $\langle \rho R \rangle$. Such asymmetric implosion is probably compatible with the asymmetric drive necessary to avoid the direct interaction of the compression beams with the cone. It is also worth observing that the configuration of the compressed core shown in Fig. 6(c) qualitatively agrees with the experiments of cone-target implosion discussed in Ref. 35.

We have also performed very simple model simulations with the Eulerian fluid code POLLUX. Again, it appears that the cone does not hinder compression substantially. However, the simulations also show sheared motion of the pellet material close to the cone surface. This aspect deserves further investigation.

Other crucial issues, so far not investigated by us, concern radiative effects, evidenced in the simulations reported in Refs. 36 and 43, as well as the development of laser irradiation schemes compatible with the cone-inserted target configuration.

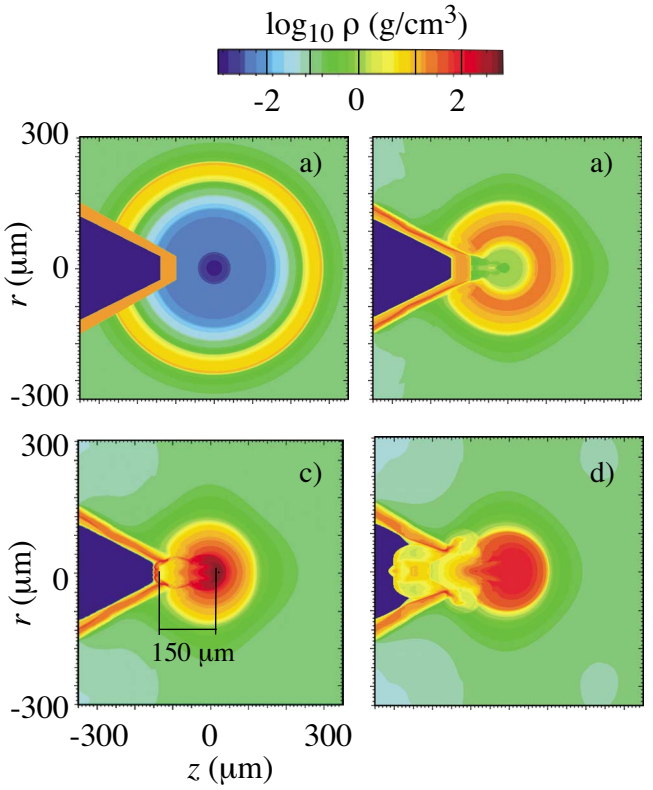

FIG. 6. (Color online) 2D simulation of a cone-guided implosion. The frames show density maps at four selected times. Frame (c) refers to the time of peak compression. Frames (c) and (d) show the approximately spherical shape of the compressed fuel.

IV. BEAM DRIVEN IGNITION

A. Model simulations and preliminary gain estimates

The ignition of the reference target was studied in Ref. 17 by DUED (Ref. 44) 2D simulations, with a 3T model, also including fusion reactions, alpha particle diffusion, and fuel depletion. The simulations assumed as initial conditions the 1D, 2T IMPLO results (density, temperatures, and velocity radial profiles) at a time close to peak compression. The actual igniting beam was replaced by a cylindrical beam (with flat intensity profiles in space and time) of particles with assigned penetration depth, straight path, and constant stopping power. It turns out that the minimum beam energy for ignition is about 18 kJ. This is achieved for a beam radius of 18–20 μm, pulse duration of about 16 ps, and particle penetration depth of 0.9–1.2 g/cm^2. Particles with longer penetration heat up a large region of fuel, while particles with shorter penetration are less effective, because a significant part of their energy is deposited in the outer lower density region of the fuel. Indeed, as clearly shown in upper frame of Fig. 7, particles generated in the low density corona, or even in the region with density about 1 g/cm^3, have to cross a layer with areal density of about 0.25 g/cm^2 before reaching the very high density region where an effective hot spot is created.

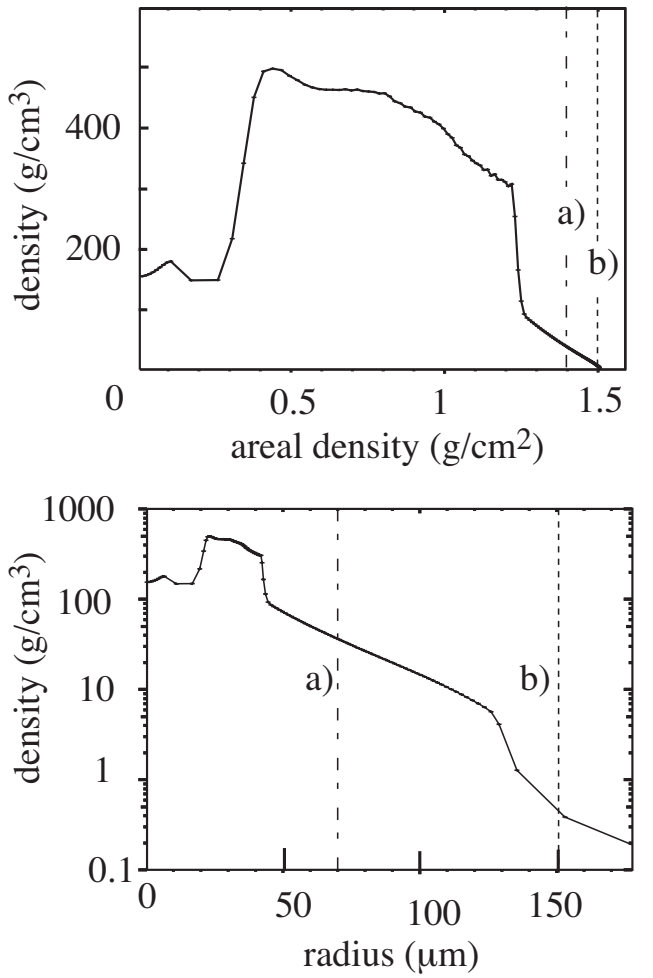

FIG. 7. Density profiles at the time of onset of electron beam interaction ($t=12.35$ ns), for the baseline target of Fig. 3 (IMPLO simulation). Upper frame: density vs areal density; lower frame: density vs radius. The dashed lines labelled (a) and (b) indicate the positions at $d_0=70$ μm and $d_0=150$ μm, respectively, where electrons are assumed to be generated in the simulations of Fig. 9 and of frames (c) and (d) of Fig. 10.

The beam intensity corresponding to the above parameters is about 0.9×10^{20} W/cm^2. Assuming $\eta_{ig}=0.25$, i.e., a four times larger laser intensity (to account for both electron generation efficiency and losses during transport from critical density to the fuel core), and using Eq. (3), the required range is obtained for $f_{\mathcal{R}}\simeq0.4$.

It was also found that the igniting beam has to be delivered in a temporal window of 75–100 ps, centered about 30–50 ps before the time of peak $\langle\rho R\rangle$.

The ignited fuel burns effectively and releases about 13 MJ of fusion energy. By combining the results of 1D IMPLO and 2D DUED simulations, in Ref. 17, it was concluded that under the (probably optimistic) assumption of coupling efficiency $\eta_{ig}=0.25$, the target of Fig. 3 could achieve a gain of 60 at total laser energy of 220 kJ. Analogous gain estimates for targets scaled at smaller and larger size lead to gains in agreement with curve (a) of Fig. 2. Using the results for compression obtained with more realistic radiation models (see Sec. II B) the gain becomes about 45 at a total energy of 300 kJ.

B. 2D simulations of the ignition of the baseline target by monoenergetic and Maxwellian electrons, including stopping and scattering

Electron stopping power depends on electron energy as well as on the properties of the stopping medium. Electron paths are deflected by collisions, and can be further affected by (self-generated) e.m. fields. In addition, laser-generated electron beams are characterized by wide energy spectra. We now describe improved studies of the ignition of fuels with HiPER relevant parameters, taking into account hot electron interaction with the plasma. We have performed two separate studies, which are presented, respectively, in the present subsection and in the following one.

A first set of simulations has been performed with DUED, now including a 3D Monte Carlo scheme for electron energy loss and scattering by the plasma. The model used includes stopping by Coulomb collisions with electrons and by the excitation of plasma waves and transverse scattering by collisions with electrons and ions. It is similar to the model used by Li and Petrasso,[45] but with the proper quantum Coulomb logarithm. When scattering is neglected, the range (and the penetration depth) of electrons with initial kinetic energy $\mathcal{E}_0$ is well approximated by

$$\mathcal{R}=\frac{\mathcal{E}_0^2}{1.96\mathcal{E}_0+1}\cdot\frac{1.5}{1-0.047\ln\rho}\ \mathrm{g/cm^2}, \tag{7}$$

with $\mathcal{E}_0$ in MeV, and the fuel density ρ in units of g/cm^3. [Equation (7) is accurate within 10% for electron energies in the interval 1 MeV$\leqslant\mathcal{E}_0\leqslant$10 MeV, and for densities up to 1000 g/cm^3. Details will be presented elsewhere.] The scaling of Eq. (7) with electron energy differs from that of Eq. (3) by a factor of $(1-1/\gamma_0)$, with γ the usual relativistic factor. At a density of 300 g/cm^3, a linear approximation to Eq. (7), centered about $\mathcal{E}_0=1.5$ MeV, is given by Eq. (3), with $f_{\mathcal{R}}=1.3$. When scattering is included, the average penetration depth decreases, and important range straggling occurs. In this case the deposition curve (versus penetration) has a broad maximum at a depth roughly in agreement with Eq. (3).

As in Ref. 17, we have simulated the ignition of the fuel of the HiPER reference target, with initial conditions from 1D, 2T IMPLO simulations at a time close to peak compression. In order to get insight, we have performed series of runs with using different physical models. First, we have neglected scattering, and considered a monoenergetic electron beam (with the same characteristics as in our previous study, namely, a cylindrical beam, generated at large distance from the target, with box intensity profile). The dashed curve in Fig. 8 shows the minimum beam energy required for ignition as a function of the electron kinetic energy. The curve has a minimum, $E_{ig}\simeq17$ kJ for electron energy of 1.5 MeV. This agrees with Ref. 17 (see also Sec. IV A above) since such electrons have a range of about 1 g/cm^2.

Next, we have considered a parallel electron beam with energy distribution $n(\mathcal{E})\propto\exp(-\mathcal{E}/k_BT)$, and therefore with average electron energy $\langle\mathcal{E}\rangle=k_BT$. The minimum ignition en-

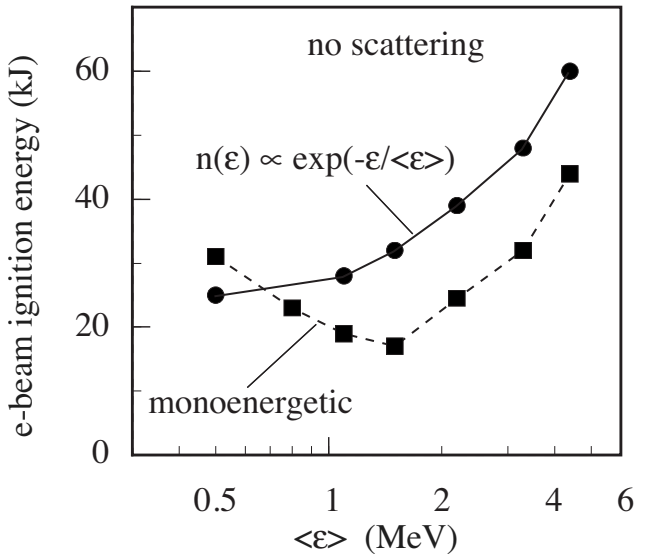

FIG. 8. From 2D simulations of the ignition of the baseline target including electron stopping, but neglecting scattering: minimum beam energy for ignition vs hot electron energy for monoenergetic electron beams (dashed curve), and electron beams with exponential energy distribution and average energy $\langle \mathcal{E} \rangle$ (solid curve).

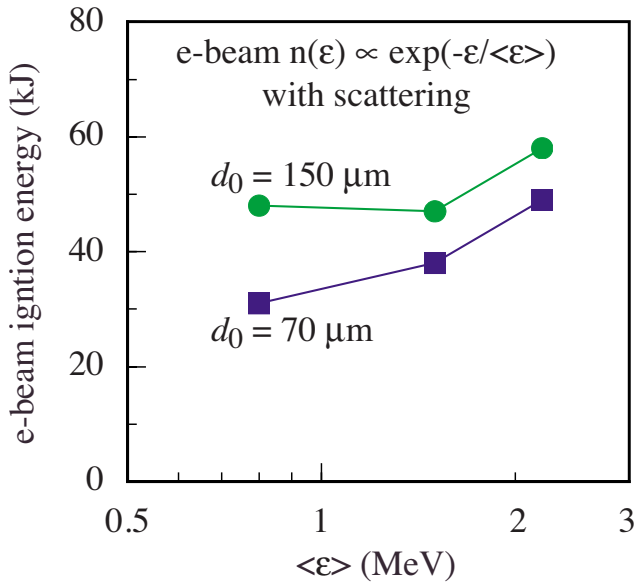

FIG. 9. (Color online) From 2D simulations of the ignition of the baseline target including electron stopping and (3D) scattering: minimum beam energy for ignition vs average electron energy, for two different values of the distance between hot electron source and fuel center.

ergies for such beams are shown by the solid curve in Fig. 8. We see that for $\langle \mathcal{E} \rangle$ in the range 1–2 MeV the ignition energy is in the range 27–38 kJ.

A final set of simulations includes electron transverse scattering (and then beam straggling and blooming). The beams are initially parallel, with Gaussian intensity profiles in space and time, and with the same exponential energy distribution as above, and are assumed to be generated at some distance d_0 from the fuel center. The larger d_0 is, the greater is the beam blooming, and hence the beam energy required for ignition. This effect is clearly seen in Fig. 9, showing the minimum ignition energy versus $\langle \mathcal{E} \rangle$ for $d=70$ μm, and $d=150$ μm, respectively. The need for generating the hot electrons as close as possible to the fuel core is evident. Figure 7 indeed shows that particles generated at $d=150$ μm have to cross a layer of plasma of depth about 100 μm, and density gradually increasing from less than 1 g/cm^3 to about 100 g/cm^3, before effectively depositing their energy.

The effects discussed above are also illustrated by Fig. 10, showing density and temperature maps at the end of the electron beam pulse, for cases just above the ignition threshold. In all cases $\langle \mathcal{E} \rangle = 1.5$ MeV. Cases (a) and (b) refer to simulations without scattering; (a) for a monoenergetic beam, (b) for a beam with exponential energy distribution $n(\mathcal{E}) \propto \exp(-\mathcal{E}/\langle \mathcal{E} \rangle)$. While in (a) all electrons are stopped at the first wall of the dense shell, in (b) the most energetic electrons cross the whole target, resulting in a diffuse preheating behind the hot spot (left-hand side of the frame). Cases (c) and (d) also include scattering; the electrons are generated at $d=70$ μm, and $d=150$ μm, in (c) and (d), respectively. In these last two cases we observe diffuse lateral fuel heating.

In the above simulations we have only considered cylindrical beams; on the other hand, we have neglected self-generated fields, which can focus (or limit defocusing of) the beam. These effects are discussed in the following subsections.

C. 2D hybrid simulation of ignition of a model fuel assembly by Maxwellian electrons, including stopping, scattering, and self-generated fields

The effect of self-generated fields has been studied by simulations with an integrated 2D code, using a hybrid (Monte Carlo and fluid) treatment.[46,47] The code also includes hydrodynamics, thermal conduction, fusion reaction, alpha particle energy deposition, and a tabulated equation-of-state.

Previous studies[20] indicate that Ohmic heating via return current prevails over direct Coulomb energy deposition at relatively low density, while it becomes negligible in the compressed core. Here no anomalous electron stopping is observed, in agreement with recent advanced particle-in-cell simulations.[48] Self-generated fields, however, can be important, because they can keep the beam collimated in the region of moderate fuel density (the halo) surrounding the core.

In order to consider a case relevant to HiPER, we have simulated the interaction of an electron beam with a DT plasma with the configuration shown in Fig. 11. It consists of a highly compressed spherical *blob*, with a peak density of 500 g/cm^3, surrounded by a low density halo, and initially at rest. It models the configuration obtained in the simulation of the cone-guided target of Fig. 6, at peak compression [frame (c)]. The imploded DT core is heated by a fast electron beam injected from the left of the simulation box, at a distance d_0 from the blob center. Laser interaction and electron beam generation inside the cone are not treated explicitly; rather the electron beam is injected at the boundary with transverse,

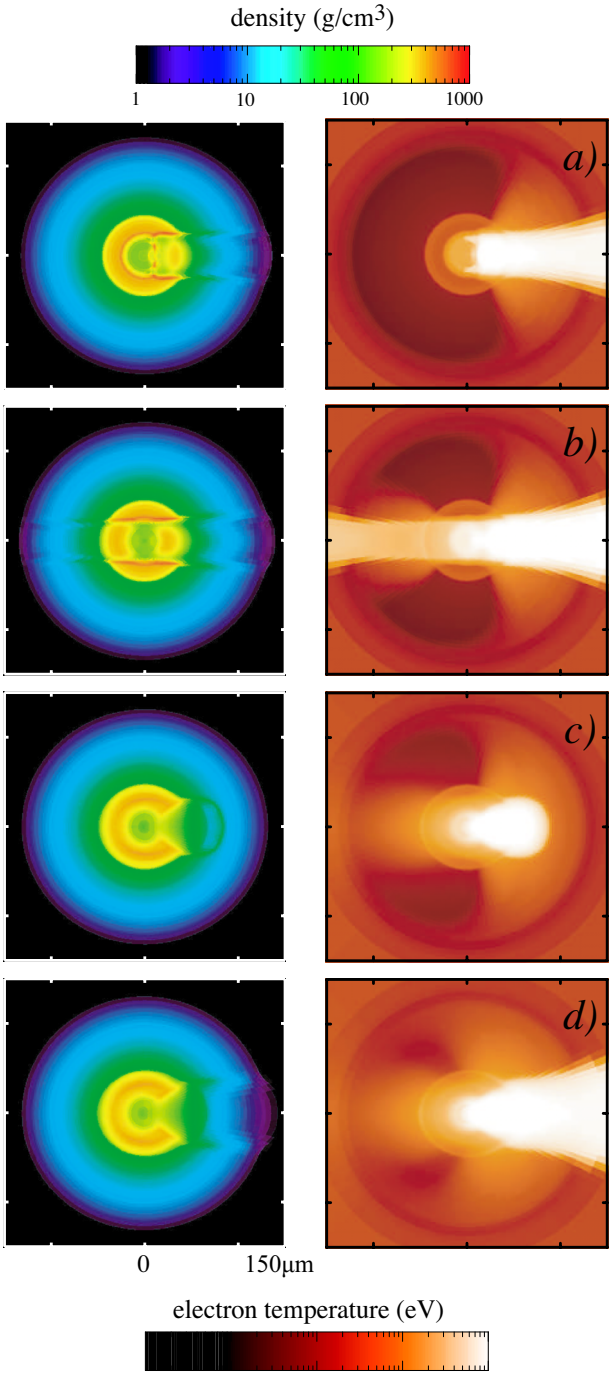

FIG. 10. (Color online) 2D DUED simulations of the ignition of the baseline target by an electron beam. Density (left column) and temperature (right) maps at the end of the electron pulse for (a) monoenergetic e-beam, square box pulse; scattering is not included in the model; (b) same as (a) but for a beam with exponential energy distribution $n(\mathcal{E}) \propto \exp(-\mathcal{E}/\langle\mathcal{E}\rangle)$; (c) beam with exponential energy distribution, Gaussian intensity profile in space and time, originating a distance $d_0=70$ μm from the fuel center; scattering is included in the simulation; (d) as (c) but for $d_0=150$ μm. In all cases the average electron energy is 1.5 MeV, while the beam energy is the minimum required for ignition: (a) $E_{ig}=17$ kJ; (b) $E_{ig}=32$ kJ; (c) $E_{ig}=38$ kJ; (d) $E_{ig}=47$ kJ.

angular, and energy distribution controlled by a few parameters.[20] We assume that the e-beam is generated by a laser beam with Gaussian profiles in radius and time. The electron energy spectrum is given by a 1D relativistic Maxwellian distribution, with temperature following the usual ponderomotive scaling [Eq. (2)]. The focal spot diameter is 40 μm (FWHM). In the simulation discussed below the average intensity is approximately 2×10^{20} W/cm^2 at 2ω ($\lambda_{ig}=0.53$ μm), laser-to-fast-electron conversion efficiency is assumed to be $\eta_{he}=0.40$. The average electron energy is about 2 MeV. For the initial beam divergence half-angle we have considered the values $\Theta=22°$, as measured in the cone-target experiments,[11,12] as well as $\Theta=30°$ and $\Theta=40°$. Pulse duration has been adjusted (typically in the interval from 10 to 20 ps) in order to achieve ignition.

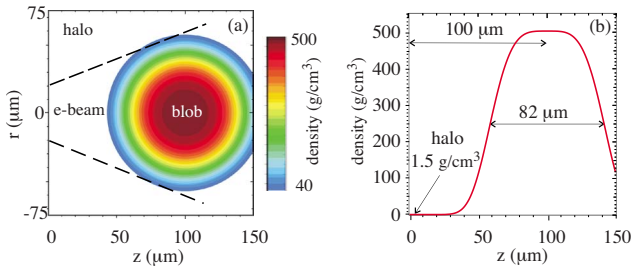

FIG. 11. (Color online) Initial fuel configuration for the hybrid model simulations of hot electron-driven fuel ignition: (a) density map (the temperature is uniform and the fuel is at rest); (b) density profile along the z-axis.

Figure 12 shows the minimum beam energy required for ignition, as a function of the distance d_0 between electron source and center of the plasma blob, for different values of the initial divergence Θ. As expected, the ignition energy grows with both Θ and d_0. It is interesting to observe that when beam-generated fields are artificially switched off the ignition energy increases substantially. This indicates that self-generated fields could help collimating the beam. They do not affect energy deposition in the compressed fuel, but are important in limiting divergence during propagation through the plasma halo. The figure shows that ignition with

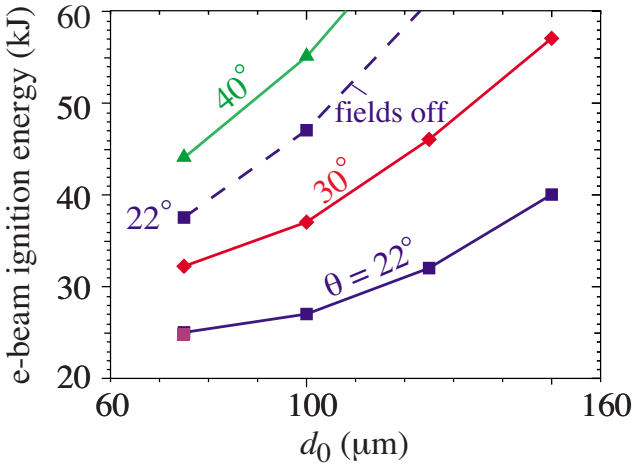

FIG. 12. (Color online) From the hybrid simulations of the ignition of the assembly of Fig. 11: electron beam ignition energy vs the distance between the electron source and the blob center, for different values of the initial beam divergence half-angle Θ. The solid curves refer to simulations including self-generated fields, while the dashed curve refers to a case with the fields artificially suppressed. Details on the beam parameters are given in the text.

laser beam energy consistent with HiPER preliminary specifications (i.e., $E_{ig} \leqslant 100$ kJ) demands low beam source divergence ($\Theta \leqslant 25°$), small values of d_0 (say, below 100 μm), as well as conversion efficiency $\eta_{he} \geqslant 40\%$.

V. CONCLUSIONS

In this paper we have discussed fast ignitor target studies performed in the framework of the HiPER project. We have used simple models and 1D and 2D numerical simulations, employing different modeling of hydrodynamics and transport. These studies have led to the identification of a baseline concept and a preliminary design of a target, and to a set of specifications for the HiPER laser beams.

It turns out that ignition and significant energy gain can be achieved with a HiPER class facility, provided certain conditions are met. First, the power of compression beams should be accurately time-tailored in order to shape the entropy profile inside the imploding shell, allowing for efficient fuel compression, while at the same time limiting the growth of the Rayleigh–Taylor instability. This is technically demanding, but otherwise tested and well understood. Concerning compression, the present improved calculations confirm general trends illustrated in Ref. 17, but indicate that the energy required to achieve the desired $\langle \rho R \rangle$ was somewhat underestimated in that study.

The crucial issue, instead, seems to be the coupling efficiency of the ultraintense beam to the compressed fuel, which must exceed 20%. This implies good conversion of the laser energy into forward directed hot electrons with penetration depth matching the optimal size of the hot spot required to trigger ignition. Using a standard scaling law [Eq. (2)] for the average energy of the hot electrons, such conditions could be met by a laser pulse with intensity somewhat in excess of 10^{20} W/cm^2, and 2ω or 3ω frequency (lower frequencies resulting in the generation of too much energetic electrons). Our simulations also clearly indicate that efficient heating also requires good collimation of the electron beam, as well as a very small distance between the region of electron generation and the compressed fuel (see Figs. 9 and 12). However, we stress that we have not simulated the interaction of the ultraintense laser pulse with the plasma and the generation of the electron beam. In particular, we have used a simple scaling law for the hot electron temperature. As discussed in Sec. II A, the dependence of this temperature on laser and plasma parameters is not yet clearly established.

Our design has been performed with the best codes at the disposal of the collaborating groups of Rome, Madrid, Bordeaux, Rutherford and London, and Lisbon. We are confident about our modeling of compression (and more generally, of hydrodynamics and energetics), of stability, and of heating and burn. On the other hand, we have not yet addressed a few crucial issues self-consistently. In addition to laser interaction, these concern, in particular, the implosion of a cone-guided target, driven by a realistic laser beam pattern, and the transport of the electron beam in a low density plasma. We believe that the experiments to be performed in the next few years at the laser facilities Omega-EP, FIREX, and PETAL,[49] supplemented by a well coordinated computational effort, will greatly contribute to addressing the electron beam generation and transport issues, reducing the uncertainties concerning the operating point of the ignition laser.

ACKNOWLEDGMENTS

This work was supported by the Italian Ministry of University and Research projects No. PRIN 2005029572, and FIRB "BLISS," by Grant No. ENE2006-06339 of the Spanish Ministry of Education, by the Aquitaine Region Council, and by the Portuguese FCT Grant No. POCI/FIS/59563/2004. S.A. thanks the Imperial College (IC), London and Rutherford Appleton Laboratory for supporting his visit to IC in Summer 2007.

[1] M. Dunne, Nature (London) **2**, 2 (2006).
[2] M. Dunne, N. Alexander, F. Amiranoff, P. Auger, S. Atzeni, H. Azechi, V. Bagnoud, P. Balcou, J. Badziak, D. Batani, C. Bellei, D. Besnard, R. Bingham, J. Breil, M. Borghesi, S. Borneis, A. Caruso, J. C. Chanteloup, R. J. Clarke, J. L. Collier, J. R. Davies, J.-P. Dufour, P. Estrailler, R. L. Evans, M. Fajardo, R. Fedosejevs, G. Figueria, J. Fils, J. L. Feugeas, M. Galimberti, J.-C. Gauthier, A. Giulietti, L. A. Gizzi, D. Goodin, G. Gregori, S. Gus'kov, L. Hallo, C. Hermandez-Gomez, D. Hoffman, J. Honrubia, S. Jacquemot, M. Key, J. Kilkenny, R. Kingham, M. Koenig, F. Kovacs, A. McEvoy, P. McKenna, J. T. Mendonca, J. Meyer-ter-Vehn, K. Mima, G. Morou, S. Moustazis, Z. Najmudin, P. Nickles, D. Neely, P. Norreys, M. Olazabal, A. Offenberger, N. Papodogianis, J. M. Perlado, J. Ramirez, R. Ramis, Y. Rhee, X. Ribeyre, A. Robinson, K. Rohlena, S. Rose, M. Roth, C. Rouyer, C. Rulliere, B. Rus, W. Sandner, A. Schiavi, G. Schurtz, A. Sergeev, M. Sherlock, L. Silva, R. Smith, G. Sorasio, C. Strangio, H. Takabe, M. Tatarakis, V. Tikhonchuk, M. Tolley, M. Vaselli, P. Velarde, T. Winstone, K. Witte, J. Wolowski, N. Woolsey, B. Wyborn, M. Zepf, and J. Zhang, HiPER—Technical Background and Conceptual Design Report 2007, Rutherford Appleton Laboratory, Report No. RAL-TR-2007-008 (June 2007), available on the site www.hiper-laser.org.
[3] M. Tabak, J. Hammer, M. E. Glinsky, W. L. Kruer, S. C. Wilks, J. Woodworth, E. M. Campbell, M. D. Perry, and R. J. Mason, Phys. Plasmas **1**, 1626 (1994).
[4] J. Lindl, *Inertial Confinement Fusion* (Springer, New York, 1998).
[5] S. Atzeni and J. Meyer-ter-Vehn, *The Physics of Inertial Fusion* (Oxford University Press, Oxford, 2004).
[6] S. Atzeni, Phys. Plasmas **6**, 3316 (1999).
[7] D. Strickland and G. Morou, Opt. Commun. **56**, 219 (1985).
[8] M. D. Perry and G. Morou, Science **264**, 917 (1994).
[9] E. M. Cambpbell, R. R. Freeman, and K. A. Tanaka (guest editors), Special Issue on Fast Ignition, Fusion Sci. Technol. **49**, 3 (2006).
[10] M. Key, Phys. Plasmas **14**, 055502 (2007).
[11] R. Kodama, P. A. Norreys, K. Mima, A. E. Dangor, R. G. Evans, H. Fujita, Y. Kitagawa, K. Krushelnick, T. Miyakoshi, N. Miyanaga, T. Norimatsu, S. J. Rose, T. Shozaki, K. Shigemori, A. Sunahara, M. Tampo, K. A. Tanaka, Y. Toyama, T. Yamanaka, and M. Zepf, Nature (London) **412**, 798 (2001).
[12] R. Kodama, H. Shiraga, K. Shigemori, Y. Toyama, S. Fujioka, H. Azechi, H. Fujita, H. Habara, T. Hall, Y. Izawa, T. Jitsuno, Y. Kitagawa, K. M. Krushelnick, K. L. Lancaster, K. Mima, K. Nagai, M. Nakai, H. Nishimura, T. Norimatsu, P. A. Norreys, S. Sakabe, K. A. Tanaka, A. Youssef, M. Zepf, and T. Yamanaka, Nature (London) **418**, 933 (2002).
[13] J. A. Delettrez, J. Myatt, P. B. Radha, C. Stoeckl, S. Skupsky, and D. D. Meyerhofer, Plasma Phys. Controlled Fusion **47**, B791 (2005).
[14] N. Miyanaga, H. Azechi, K. A. Tanaka, T. Kanabe, T. Jitsuno, Y. Fujimoto, R. Kodama, H. Shiraga, K. Kondo, K. Tsubakimoto, Y. Kitagawa, H. Fujita, S. Sakabe, H. Yoshida, K. Mima, T. Yamanaka, and Y. Yzawa, in *Inertial Fusion Sciences and Applications 2003*, edited by B. Hammel, D. D. Meyerhofer, J. Meyer-ter-Vehn, and H. Azechi (American Nuclear Society, Lagrange Park, Illinois, 2004), p. 507.
[15] B. Hammel and the National Ignition Campaign Team, Plasma Phys. Controlled Fusion **48**, B497 (2006).
[16] C. Cavailler, Plasma Phys. Controlled Fusion **47**, B389 (2005).
[17] S. Atzeni, A. Schiavi, and C. Bellei, Phys. Plasmas **14**, 052702 (2007).

[18]R. Betti, A. A. Solodov, J. A. Delettrez, and C. Zhou, Phys. Plasmas **13**, 100703 (2006).
[19]A. A. Solodov, R. Betti, J. A. Delettrez, and C. D. Zhou, Phys. Plasmas **14**, 062701 (2007).
[20]J. J. Honrubia and J. Meyer-ter-Vehn, Nucl. Fusion **46**, L25 (2006).
[21]R. G. Evans, Plasma Phys. Controlled Fusion **49**, B87 (2007).
[22]M. Tabak, D. Hinkel, S. Atzeni, E. M. Campbell, and K. Tanaka, Fusion Sci. Technol. **49**, 254 (2006).
[23]S. Atzeni and M. Tabak, Plasma Phys. Controlled Fusion **47**, B769 (2005).
[24]S. C. Wilks, W. L. Kruer, M. Tabak, and A. B. Langdon, Phys. Rev. Lett. **69**, 1383 (1992).
[25]G. Malka and J. L. Miquel, Phys. Rev. Lett. **77**, 75 (1996).
[26]F. N. Beg, A. R. Bell, A. E. Dangor, C. N. Danson, A. P. Fews, M. E. Glinsky, B. A. Hammel, P. Lee, P. A. Norreys, and M. Tatarakis, Phys. Plasmas **4**, 447 (1997).
[27]F. Pisani, A. Belardinello, D. Batani, A. Antonicci, E. Martinolli, M. Koenig, L. Gremillet, F. Amiranoff, S. Baton, J. Davies, T. Hall, D. Scott, P. Norreys, A. Djaoui, C. Rosseaux, P. Fews, H. Bandulet, and H. Pepin, Phys. Rev. E **62**, R5927 (2000).
[28]S. C. Wilks and W. L. Kruer, IEEE J. Quantum Electron. **33**, 1954 (1997).
[29]Y. Sentoku, Bull. Am. Phys. Soc. **52**, 269 (2007).
[30]R. R. Freeman, D. Batani, S. Baton, M. Key, and R. Stephens, Fusion Sci. Technol. **49**, 297 (2006).
[31]R. Betti and C. Zhou, Phys. Plasmas **12**, 110702 (2005).
[32]W. L. Kruer, *The Physics of Laser Plasma Interactions* (Addison-Wesley, New York, 1988).
[33]K. Anderson and R. Betti, Phys. Plasmas **11**, 5 (2004).
[34]S. Atzeni, Plasma Phys. Controlled Fusion **29**, 1535 (1987).
[35]R. B. Stephens, S. P. Hatchett, R. E. Turner, K. A. Tanaka, and R. Kodama, Phys. Rev. Lett. **91**, 185001 (2003).
[36]S. P. Hatchett, D. Clark, M. Tabak, R. E. Turner, C. Stoeckl, R. B. Stephens, H. Shiraga, and K. Tanaka, Fusion Sci. Technol. **49**, 327 (2006).
[37]S. Slutz and M. C. Herrmann, Phys. Plasmas **10**, 234 (2003).
[38]J. J. Honrubia, J. Quant. Spectrosc. Radiat. Transf. **49**, 491 (1993).
[39]P.-H. Maire, R. Abgrall, J. Breil, and J. Ovadia, SIAM J. Sci. Comput. (USA) **29**, 1781 (2008).
[40]M. Olazabal-Loumé and L. Hallo, Phys. Plasmas **14**, 102705 (2007).
[41]X. Ribeyre, Ph. Nicolaï, G. Schurtz, M. Olazabal-Loumé, J. Breil, P. H. Maire, J. L. Feugeas, L. Hallo, and V. T. Tikhonchuck, Plasma Phys. Controlled Fusion **50**, 025007 (2007).
[42]G. J. Pert, J. Comput. Phys. **43**, 111 (1981).
[43]H. Nagatomo, T. Johzakhi, T. Nakamura, H. Sagakami, A. Sunahara, and K. Mima, Phys. Plasmas **14**, 056303 (2007).
[44]S. Atzeni, A. Schiavi, F. Califano, F. Cattani, F. Cornolti, D. Del Sarto, T. V. Liseykina, A. Macchi, and F. Pegoraro, Comput. Phys. Commun. **169**, 153 (2005), and references therein.
[45]C. K. Li and R. D. Petrasso, Phys. Plasmas **13**, 056314 (2006).
[46]A. R. Bell, J. R. Davies, S. Guerin, and H. Ruhl, Plasma Phys. Controlled Fusion **39**, 653 (1997).
[47]J. R. Davies, Phys. Rev. E **68**, 056404 (2003).
[48]A. J. Kemp, Y. Sentoku, V. Sotnikov, and S. C. Wilks, Phys. Rev. Lett. **97**, 235001 (2006).
[49]N. Blanchot, G. Marre, J. Nauport, E. Sib, C. Rouyer, S. Montant, A. Cotel, C. Le Blanc, and C. Sauteret, Appl. Opt. **45**, 6013 (2006).